

NAG5-332

RECEIVED
CONTRACTS AND GRANTS

73 pages

AUG 10 12 30 PM '84

FT 889400 IN-11568

THE FLORIDA STATE UNIVERSITY
COLLEGE OF ARTS AND SCIENCES

A MODEL FOR THE ESTIMATION OF THE SURFACE FLUXES OF
MOMENTUM, HEAT, AND MOISTURE OF THE CLOUD
TOPPED MARINE ATMOSPHERIC BOUNDARY LAYER
FROM SATELLITE MEASURABLE PARAMETERS

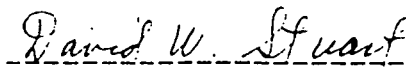
by

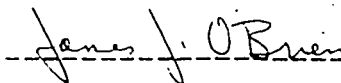
DONALD EUGENE ALLISON

A Thesis submitted to the
Department of Meteorology
in partial fulfillment of the
requirements for the degree of
Master of Science

Approved:


Professor Directing Thesis





August, 1984

(NASA-CR-177283) A MODEL FOR THE ESTIMATION
OF THE SURFACE FLUXES OF MOMENTUM, HEAT AND
MOISTURE OF THE CLOUD TOPPED MARINE
ATMOSPHERIC BOUNDARY LAYER FROM SATELLITE
MEASURABLE PARAMETERS (Florida State Univ., G3/46

N86-27837

Unclas
43228

ABSTRACT

This thesis develops a model for the estimation of the surface fluxes of momentum, heat, and moisture of the cloud topped marine atmospheric boundary layer by use of satellite remotely sensed parameters. The parameters chosen for the problem are the integrated liquid water content, q_{li} , the integrated water vapor content, q_{vi} , the cloud top temperature, the sea surface temperature, and either a measure of the 10 meter neutral wind speed or the friction velocity at the surface.

Under the assumptions of a horizontally homogeneous, well-mixed boundary layer, the model calculates the equivalent potential temperature and total water profiles of the boundary layer along with the boundary layer height from inputs of q_{li} , q_{vi} , and cloud top temperature. These values, along with the 10m neutral wind speed or friction velocity and the sea surface temperature, are then used to estimate the surface fluxes using the methods of Stage (1979) and Liu, Katsaros, and Businger (1979).

The development of a scheme to parameterize the integrated water vapor outside of the boundary layer for

the cases of cold air outbreak and California coastal stratus is presented. The scheme involves the mean profiles of relative humidity and temperature along with the mean jump of potential temperature through the inversion to calculate the integrated water vapor. In turn, this leads to a method of calculating the radiative temperature flux at the cloud top by use of Staley and Jurica's (1970, 1972) radiation model.

Sensitivity studies are presented showing the potential accuracy of the technique. The model's expected accuracies with existing satellite technology are 24% for the heat flux and 82% for the moisture flux. However, these expected errors will be reduced with improvement of the satellite parameter retrieval algorithms.

In conclusion, with improvements of current technology, the model will provide reasonable estimates of the surface fluxes. The model is the only one of its kind currently available to estimate the surface fluxes of momentum, heat, and moisture of the cloud topped marine atmospheric boundary layer from satellite measurable parameters.

DEDICATION

This thesis and the work that went into it was made possible by the incredible patience shown towards me by my fiancée, Lori, and my family, and it is to these people whom I dedicate this.

ACKNOWLEDGEMENTS

This thesis was made possible by the support given to me through the traineeship offered by NASA through the Florida State University. The topic discussed in this thesis was suggested by Dr. Steven A. Stage through his own work under NASA grant NAG 5-332.

My thanks to Dr. Steven A. Stage whose guidance and support have been indispensable. My thanks also to Dr. James J. O'Brien, Head of the NASA traineeship program, whose mental and financial support has allowed me to complete my graduate program. Thanks are also given to Dr. David W. Stuart whose lunchtime discussions kept me in touch with the real world outside of the university. My thanks to all of these gentlemen for the suggestions they made for the improvement of this work.

Lastly, a very special thank you to my parents and my fiancée, Lori, for all that they have done during my pursuit of education.

TABLE OF CONTENTS

	Page
LIST OF TABLES.	vii
LIST OF FIGURES	viii
 Chapter	
1 INTRODUCTION.	1
1.1 Purpose	1
1.2 Scientific Importance of Cold Air Outbreak.	2
1.3 The Model	3
1.4 Satellite Technology.	4
2 MODEL DEVELOPMENT	6
2.1 Introduction.	6
2.2 Basic Variables and Thermodynamics.	10
2.3 Derivation of Model's Equations	14
2.4 Inversion of Equations.	19
2.5 Calculation of Surface Fluxes	26
2.6 Parameterizing Water Vapor Above the MABL	37
2.7 Radiative Flux.	39
3 COMPUTATIONAL FORM OF THE MODEL	41
3.1 Introduction.	41
3.2 The Model	41
4 MODEL RESULTS	45
4.1 Introduction.	45
4.2 Model Applications.	45
4.3 Variation of Input and Output Parameters.	46
4.4 Expected Model Accuracies with Satellite Data	58
4.5 Strengths and Weaknesses.	61
5 CONCLUSIONS	63
REFERENCES.	65

LIST OF TABLES

Number		Page
2.5.1	The Lower Boundary Values of the Logarithmic Profiles $z_{tu}/=a_1 R^{b_1}$ and $z_{qu}/=a_2 R^{b_2}$. . .	31
4.4.1	Individual Expected Errors due to Each Satellite Parameter and Total Expected Model Error	60

LIST OF FIGURES

Number		Page
2.1.1	Atmospheric Cross Section with Oversized Marine Atmospheric Boundary Layer: Arrows Pointing Down Indicate Satellite Measurable Parameters, Arrows Pointing Up Indicate Fluxes	7
2.1.2	Marine Atmospheric Boundary Layer Profiles of Θ_e and q_t	8
2.1.3	Model Flowchart Showing Steps Necessary to Estimate the Fluxes	9
2.3.1	Profile of q_1 in Marine Boundary Layer. . . .	18
2.4.1	Profile of q_1 in Marine Boundary Layer with Fog.	23
4.3.1	Variation of Heat Flux with Cloud Top Temperature	49
4.3.2	Variation of Moisture Flux with Cloud Top Temperature	50
4.3.3	Variation of Heat Flux with Sea Surface Temperature	51
4.3.4	Variation of Moisture Flux with Sea Surface Temperature	52
4.3.5	Variation of Heat Flux with Integrated Liquid Water Content	54
4.3.6	Variation of Moisture Flux with Integrated Liquid Water Content.	55
4.3.7	Variation of Heat Flux with Integrated Water Vapor Content	56
4.3.8	Variation of Moisture Flux with Integrated Water Vapor Content	57

CHAPTER 1 : INTRODUCTION

1.1 PURPOSE

The purpose of this thesis is to develop a model for the estimation of the surface fluxes of momentum, heat, and moisture by use of satellite remotely sensed parameters of the cloud-topped marine atmospheric boundary layer.

The thesis first introduces the problem. Second, the equations used to solve the problem are shown. Third, the computational form of the model is presented. Fourth, the results of the test runs of the model are given. Last, the thesis conclusions are drawn.

The satellite parameters chosen for this problem are the integrated liquid water content of the atmosphere, the integrated water vapor content of the atmosphere, the cloud top temperature, the sea surface temperature, and either a measurement of the 10 meter neutral wind speed or the friction velocity at the surface. This set of parameters is not the only possible set, but the technology exists today to remotely sense this set; hence,

it was chosen for this study. The current technology to measure this set is discussed later in this chapter, but first the importance of this study is considered.

1.2 SCIENTIFIC IMPORTANCE OF COLD-AIR OUTBREAK

Modelling of the air-sea surface fluxes of momentum, heat, and moisture by use of remotely sensed satellite parameters is of importance due to the effect these fluxes have on the regional and global weather.

Cold air outbreak has a pronounced effect on the western sections of midlatitude oceans off the east coasts of Asia and North America. In these regions, high winds, large air-sea temperature differences, and relatively dry air combine to give heat and moisture fluxes which are much greater than oceanic means. These fluxes over the warm water currents of the Kuroshio and Gulf Stream are known to have profound effects on cyclogenesis and storm intensification, particularly on the development of wintertime cyclones from Taiwan and Cape Hatteras lows (Chou and Atlas, 1982; Agee and Howley, 1977).

Recently, a method has been suggested by Chou and Atlas (1982) and Stage (1983) to estimate the heat and moisture surface fluxes in the region between the shore

and the edge of a cloud bank during cold air outbreak, by remotely sensed parameters. This method uses the boundary layer model developed by Stage and Businger (1981 a,b) for cold air outbreak. Further research is needed; however, to extend the estimation of the fluxes into the cloudy region. Hence, the reason for this study is the need of a model to estimate the surface fluxes in the cloudy region.

1.3 THE MODEL

The model developed in this study is capable of estimating the surface fluxes of momentum, heat, and moisture during a cold air outbreak by use of remotely sensed parameters of the marine atmospheric boundary layer. This model is based on the models of Stage (1979) and Liu, et al. (1979). It assumes unstable boundary layer conditions and uses the Businger diabatic profiles. Because of the assumption of unstable conditions, the model is not valid in neutral or stable conditions. However, the large air-sea temperature differences common in cold air outbreak or the large cloud top radiative temperature fluxes seen in California coastal stratus cases both produce the well-mixed boundary layer

conditions needed for the model to run. The model is also limited by the presence of fog. Although the model has been revised to include the presence of advection fog, it is still unclear as to how the equations which calculate the surface fluxes react in foggy conditions. Hence, fog is an area in which further study is necessary.

1.4 SATELLITE TECHNOLOGY

The technology exists today to measure the parameters: cloud top temperature, integrated water vapor content, integrated liquid water content, sea surface temperature, and either a 10m neutral wind speed or a friction velocity for use in this model to estimate the surface fluxes.

Cloud top temperature may be obtained from infrared satellite measurements, such as the infrared sensors on the GOES east and west satellites. The other parameters may be calculated by use of a scanning multichannel microwave radiometer (SMMR) such as the one carried aboard SEASAT or the one currently aboard NIMBUS 7.

The SMMR instrument's primary purpose is to measure sea surface temperature and to provide a measurement of the surface wind speed. However, SMMR also provides

estimates of atmospheric water vapor and liquid water contents. The latter two parameters are found by scanning over various channels and employing an algorithm developed by Chang and Wilheit (1979). An survey of SMMR's capabilities may be found in the book, Satellite Microwave Remote Sensing, edited by T.D. Allan (1983).

As one can see, with existing technology the parameters needed for this model may be estimated from satellite measurements. In the next chapter, the model development is discussed.

CHAPTER 2 : MODEL DEVELOPMENT

2.1 INTRODUCTION

The model development is discussed in this chapter. As stated in the first chapter, the purpose of the model is to estimate the surface fluxes of momentum, heat, and moisture. One method of accomplishing this task is to find an estimate of the variables θ_e , q_t , and z_b (See Figure 2.1.1). This may be done with satellite measurements of θ_b , q_{li} , and q_{vi} , and assuming an unstable, well mixed boundary layer with θ_e and q_t being conserved quantities (See Figure 2.1.2). Then, with an estimate of the neutral wind speed or the friction velocity and the sea surface temperature, the surface fluxes may be found by using the bulk aerodynamic formulas (See Figure 2.1.3).

First in this chapter, some basic variables and thermodynamics are introduced. Second, the derivation of equations for the model are shown. Third, the model equations are inverted. Fourth, the equations used to estimate the surface fluxes are shown. Fifth, the

ORIGINAL PAGE IS
OF POOR QUALITY

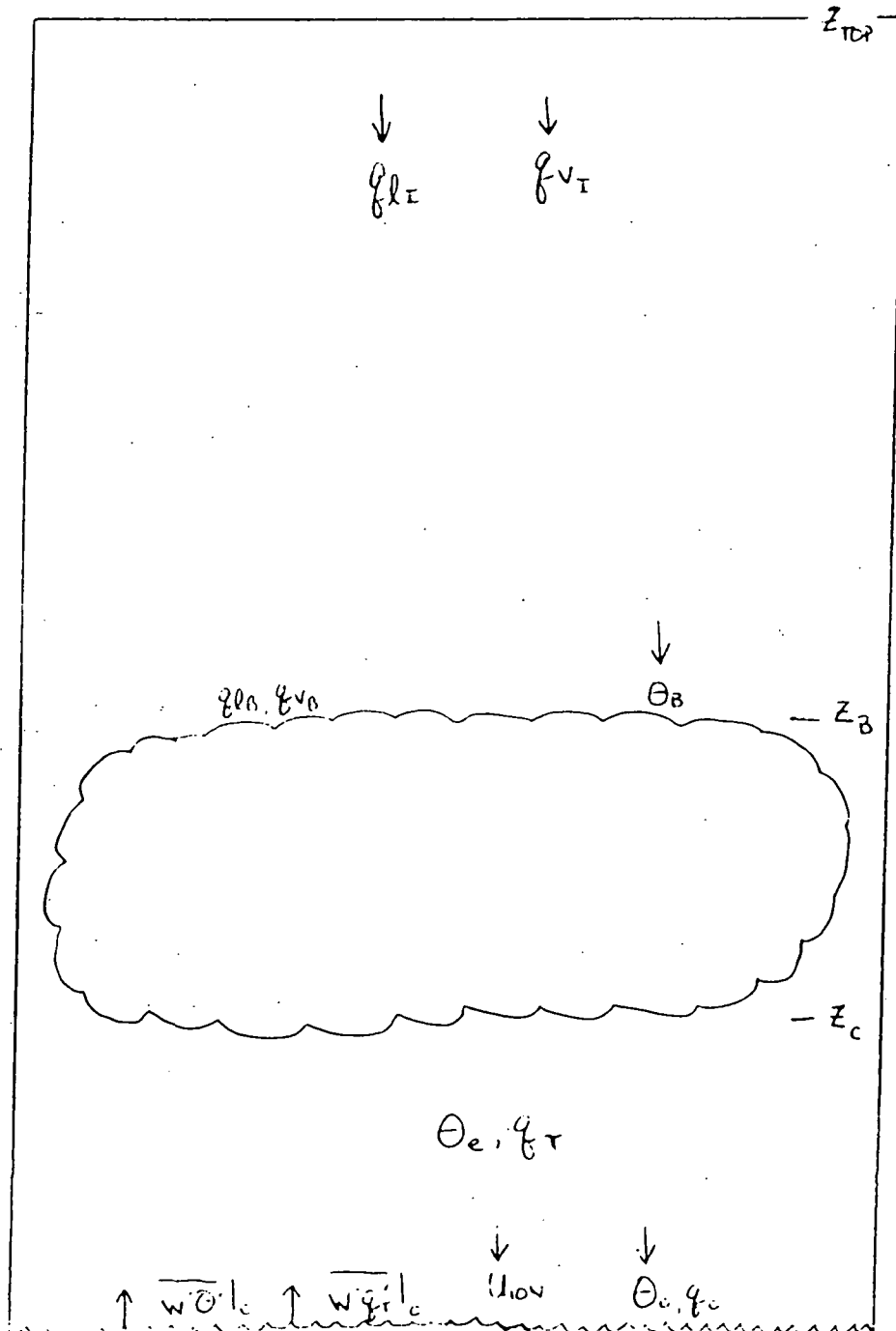


Figure 2.1.1. Atmospheric Cross Section with Oversized Marine Atmospheric Boundary Layers: Arrows Pointing Down Indicate Satellite Measurable Parameters, Arrows Pointing Up Indicate Fluxes

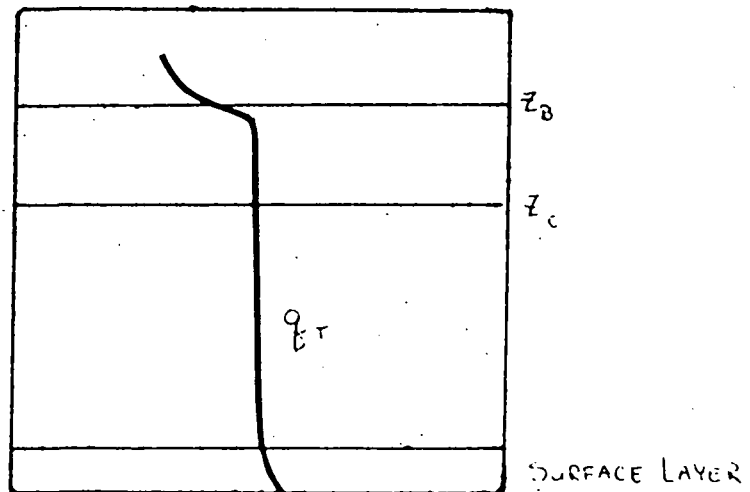
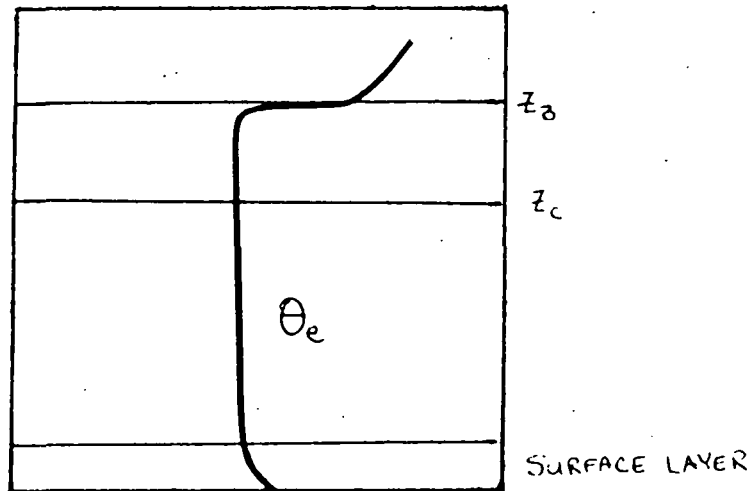


Figure 2.1.2. Marine Atmospheric Boundary Layer Profiles of Θ_e and q_t

ORIGINAL PAGE IS
OF POOR QUALITY

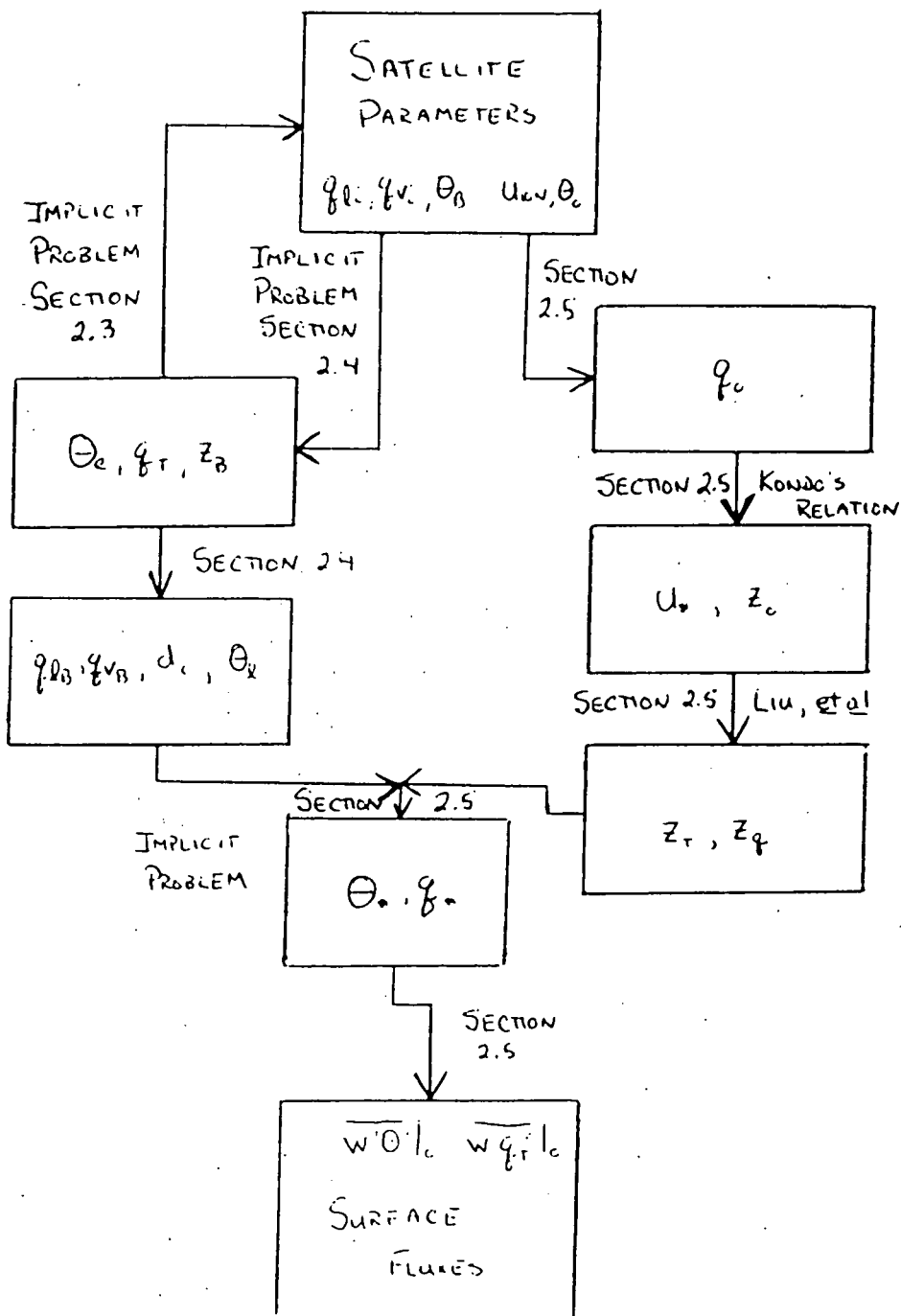


Figure 2.1.3. Model Flowchart Showing Steps Necessary to Estimate the Fluxes

parameterization of the liquid and water vapor contents outside of the boundary layer is presented. Last, a method to calculate the radiative temperature flux at cloud top is discussed.

2.2 BASIC VARIABLES AND THERMODYNAMICS

The basic variables used in this paper are now introduced.

T_d	Dewpoint temperature
Θ	Potential temperature
Θ_0	Sea surface temperature
Θ_b	Cloud top temperature
q_t	Total water mixing ratio
q_{vb}	Water vapor mixing ratio at cloud top
q_{lb}	Liquid water mixing ratio at cloud top
z_b	Cloud top height
z_c	Cloud base height
z_s	Saturation level height
k	von Karman's constant
ϵ	Ratio of molecular weights of water and air

The basic thermodynamic properties are now shown. The equivalent potential temperature may be approximated

by

$$\theta_e = \theta + (L_v / C_p) q_v \quad (2.2.1)$$

where L_v is the latent heat of evaporation for water and C_p is the specific heat of air at constant pressure. The total water mixing ratio is defined as

$$q_t = q_v + q_l \quad (2.2.2)$$

The Clausius-Clapeyron equation may be written as

$$de = [(e L_v \epsilon) / ((T_d^2) R)] dT_d \quad (2.2.3)$$

where e is the water vapor partial pressure and ϵ is taken as 0.622. The water vapor partial pressure is related to the mixing ratio by

$$q_v = (\epsilon / p) e \quad (2.2.4)$$

where p = atmospheric pressure. The differential of (2.2.4) gives

$$(dq_v/q_v) = (de/e) - (dp/p) \quad (2.2.5)$$

Substituting the hydrostatic equation $dp/dz = -\rho g$, the perfect gas law, $p = \rho RT$, and (2.2.3) into (2.2.5) gives

$$(dq_v/q_v) = (L_v \epsilon / (T_d^2 R)) dT_d + (g / (RT)) dz \quad (2.2.6)$$

Now, (2.2.6) may be integrated if one knows the saturation mixing ratio, q_r , corresponding to some dewpoint temperature, T_{dr} , allowing the defining of two functions:

$$Q(T) = q_r \exp[(-L_v \epsilon / R)(1/T - 1/T_{dr})] \quad (2.2.7)$$

and

$$T_{dew}(q) = [R / (L_v \epsilon) \ln(q/q_r) + 1/T_{dr}]^{-1} \quad (2.2.8)$$

Thus, $Q(T)$ is the saturation mixing ratio for air at $z=0$, with temperature, T ; and $T_{dew}(q)$ is the dewpoint for air at $z=0$, with water vapor mixing ratio, q . These two functions are inverses; therefore,

$$T = T_{\text{dew}}(Q(T)) \quad (2.2.9a)$$

and

$$q = Q(T_{\text{dew}}(q)) \quad (2.2.9b)$$

In order to evaluate these functions, Stage (1979) obtained saturation vapor pressures from the Smithsonian Meteorological Tables. He chose values to give the best fit for the temperature range between 0 and 10 °C. This gives the function as

$$Q(T) = 5.3542 \times 10^{-3} (\exp[-5399.286(1/T - 3.59505 \times 10^{-3})]) \quad (2.2.10)$$

and

$$T_{\text{dew}}(q) = 5399.286 / [21.0640 - \ln(q \times 10^3)] \quad (2.2.11)$$

where T and T_{dew} are in Kelvin and q and Q are in g/kg. The liquid water potential temperature may be defined as

$$\theta_1 = \theta_e - (L_v / C_p) q_t \quad (2.2.12)$$

and since θ_e and q_t are conserved in non-precipitating, no

ice, parcel motion, θ_1 is also a conserved quantity. Below the saturation level, $q_1=0$, and $\theta_1 = \theta$. The saturation level or lifting condensation level is expressed as

$$z_s = (\theta_1 - T_{d0}) / (\gamma - (gT)/(L_v \epsilon)) \quad (2.2.13)$$

where γ is the dry adiabatic lapse rate and $(gT)/(L_v \epsilon)$ may be expressed as the lapse rate of dewpoint. The last thermodynamic property to be introduced is the virtual potential temperature, θ_v .

$$\theta_v = \theta (1 + (1/\epsilon - 1)q_v - q_1) \quad (2.2.14)$$

Virtual potential temperature introduces the effects of both the buoyancy of water vapor and liquid water drag.

2.3 DERIVATION OF MODEL'S EQUATIONS

The equations used in this model were developed for the case of cold air outbreak. The marine atmospheric boundary layer (MABL) is assumed to be cloud topped and well mixed with θ_e and q_t being conserved quantities. The

cloud base is assumed to be equal to the saturation level and that all motions in the cloud layer are saturated. The cloud top is assumed to be equivalent to the base of the inversion layer.

A method is needed to determine values for the cloud top temperature, Θ_b , the integrated liquid water content, q_{li} , and the integrated water vapor content, q_{vi} , of the marine boundary layer. The marine boundary layer model developed by Stage (1979) provides such a method. Stage incorporates a routine to handle saturated partial behavior in which inputs of Θ_e and z_b produce values of Θ_v and q_v for a saturated parcel. Hence, with inputs of Θ_e , q_t , and z_b it is possible to find Θ_b , q_{li} , and q_{vi} .

A method is now shown in which the cloud top temperature may be estimated by use of an iterative method with initial inputs of Θ_e , q_t , and z_b , and an initial guess for Θ_b .

Cloud top temperature may be found by use of the following equations.

$$T_{db} = \Theta_b - (\delta - (gT)/(L_v \epsilon)) z_b \quad (2.3.1)$$

The water vapor mixing ratio at cloud top may be found by using (2.2.9b) and (2.3.1) where

$$q_{vb} = Q(T_{db}) \quad (2.3.2)$$

From (2.3.2) it follows that

$$dq_{vb} = dQ/dT [d\theta_b - (\gamma - (qT)/(L_v \xi)) dz_b] \quad (2.3.3)$$

The finite difference form of (2.3.3) is

$$dQ/dT = [Q(T_{db} + \Delta T) - q_{vb}] / \Delta T \quad (2.3.4)$$

where ΔT is a small increment. The quantity, $\delta\theta_b$, is expressed as

$$\delta\theta_b = [\theta_e - (\theta_b + (L_v/C_p) q_{vb})] / [1 + (L_v/C_p) dQ/dT] \quad (2.3.5)$$

Therefore, by making an initial guess at θ_b , one may use equations (2.3.1) to (2.3.5) and

$$\theta_{bnew} = \theta_{bold} + \delta\theta_b$$

one may iterate numerically until a suitably small $\delta\theta_b$ is reached, thus providing θ_b and q_{vb} .

The liquid water mixing ratio at cloud top may be found from

$$q_{1b} = q_t - q_{vb} \quad (2.3.6)$$

In order to solve for the integrated liquid water content, q_{1i} , the depth of the cloud layer, d_c must be found. Using equations (2.2.12), for θ_1 , and (2.2.13), for z_s , and assuming that z_s , the saturation level, is equal to z_c , the cloud base level

$$d_c = z_b - z_c \quad (2.3.7)$$

Below cloud base, $q_1 = 0$. The liquid water mixing ratio is assumed to increase linearly with height from z_c to z_b , and then is assumed to be equal to zero above the boundary layer (See Figure 2.3.1).

Thus the q_1 profile in the cloud layer forms a triangle, and the integrated liquid water content may be found by

$$q_{1i} = 0.5 \times q_{1b} \times d_c \quad (2.3.8)$$

The integrated total water content, q_{ti} , of the boundary

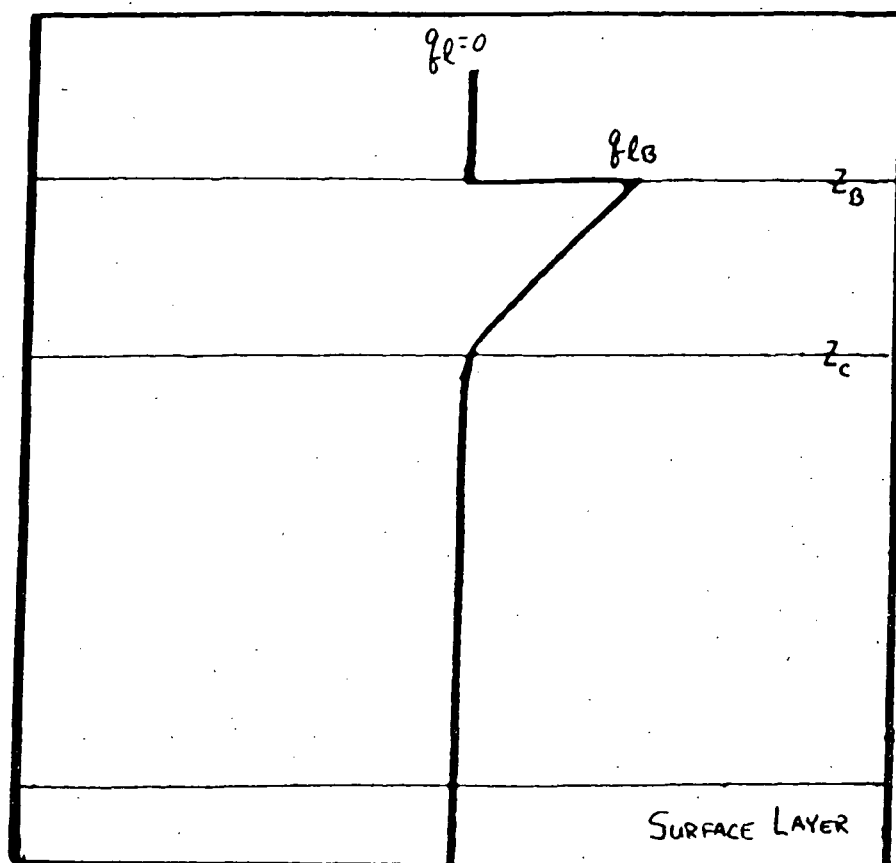


Figure 2.3.1. Profile of q_l in Marine Boundary Layer

layer is expressed as

$$q_{ti} = \int_0^{z_b} q_t dz$$

Since q_t is well mixed in the boundary layer

$$q_{ti} = q_t \times z_b \quad (2.3.9)$$

Hence the final quantity, the integrated water vapor content, may be found

$$q_{vi} = q_{ti} - q_{li} \quad (2.3.10)$$

Now that the quantities, Θ_b , q_{li} , and q_{vi} have been derived, the problem may be inverted.

2.4 INVERSION OF EQUATIONS

The previous section showed a method in which with inputs of Θ_s , q_t , and z_b were used to find the satellite parameters Θ_b , q_{li} , and q_{vi} . In order to compute the boundary layer profiles from these satellite parameters a numerical method must be found to invert the set of

equations in the last section. By inverting the equations in Section 2.3 allows one to take the satellite measurable data and calculate z_b and the boundary layer profiles of θ_e and q_t . To begin, the satellite measurable parameters, q_{li} , q_{vi} , and θ_b are used as input. Then one may calculate

$$q_{ti} = q_{vi} + q_{li} \quad (2.4.1)$$

It is also possible to express q_{ti} as

$$q_{ti} = \int_{z_b}^{z_{top}} q_t dz + \int_0^{z_b} q_t dz$$

Taking $\int_{z_b}^{z_{top}} q_t dz$ as a known quantity, this will be discussed in Section 2.6, and taking $q_t = \text{constant}$ below z_b one may write

$$q_{ti} = \int_{z_b}^{z_{top}} q_t dz + q_t \times z_b$$

where

$$q_t \times z_b = q_{ti} - \int_{z_b}^{z_{top}} q_t dz \quad (2.4.2)$$

We now have the quantity $(q_t \times z_b)$ from which q_t and z_b may

be found by guessing z_b and solving for q_t . Then, by use of the following set of equations and a *regula falsi* method, it is possible to estimate the variables θ_e , q_t , and z_b which are needed in the flux calculations.

By guessing z_b and solving

$$q_t = (q_t \times z_b) / z_b \quad (2.4.3)$$

one is left with q_t and z_b . From equation (2.3.1) one gets

$$T_{db} = \theta_b - (\gamma - (gT) / (L_v \epsilon)) z_b \quad (2.4.4)$$

The water vapor mixing ratio may be found by

$$q_{vb} = Q(T_{db}) \quad (2.4.5)$$

Where $Q(T)$ is the function described by equation (2.2.10).

The equivalent potential temperature, θ_e , is found from equation (2.2.1)

$$\theta_e = \theta_b + (L_v / C_p) q_{vb} \quad (2.4.6)$$

The liquid water mixing ratio at cloud top is

$$q_{lb} = q_t - q_{vb} \quad (2.4.7)$$

The dewpoint just above the sea surface may be found from

$$T_{d0} = T_{dew}(q_t) \quad (2.4.8)$$

Where $T_{dew}(q)$ is the function expressed by equation (2.2.11). The liquid water potential temperature comes from equation (2.2.12)

$$\theta_1 = \theta_s - (L_v / C_p) q_t \quad (2.4.9)$$

The saturation level may be calculated using equation (2.2.13)

$$z_s = (\theta_1 - T_{d0}) / (\gamma - (gT) / (L_v \epsilon)) \quad (2.4.10)$$

If z_s is greater than z_b , no cloud is formed in the model, and the model ends. If z_s is less than zero, then fog is present below cloud level. In the case of fog, q_{l1} , is no longer proportional to the area of the triangle shown in Figure 2.3.1. The trapezoidal rule can now be applied as

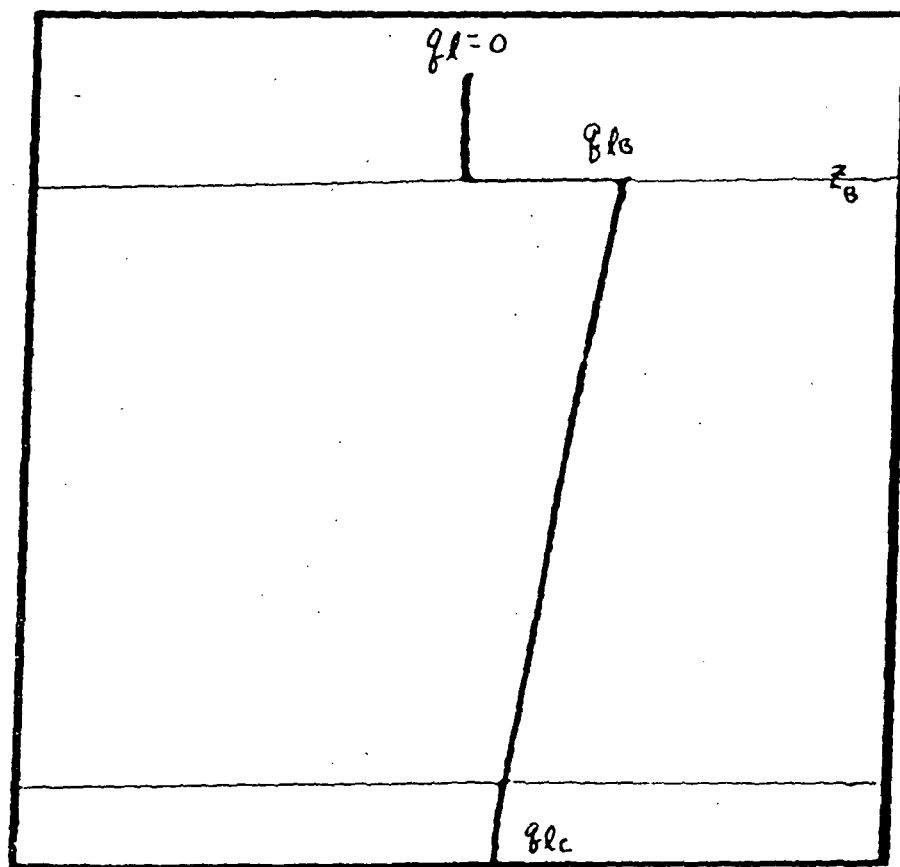


Figure 2.4.1. Profile of q_1 in Marine Boundary Layer with Fog

can be seen in Figure 2.4.1.

The value of q_1 at the cloud base is called q_{1c} . Under no fog conditions, $q_{1c}=0$. In the case of fog, the cloud base is at the surface and q_{1c} is not equal to zero. Note that the term "fog" refers to advection fog. If fog is present in the boundary layer, q_{1c} may be found from the input values of θ_s , q_t , and z_s by the same iterative method shown in Section 2.3.

The dewpoint temperature at z_s may be found by

$$T_{ds} = \theta_s - (\gamma - (qT)/(L_v \epsilon)) z_s \quad (2.4.11)$$

where a value for θ_s has been guessed. The water vapor mixing ratio at saturation level is

$$q_{vs} = Q(T_{ds}) \quad (2.4.12)$$

where $Q(T)$ is from equation (2.2.10). A small increment, ΔT , is now introduced in which

$$T_{dsnew} = T_{dsold} + \Delta T \quad (2.4.13)$$

The mixing ratio of T_{dsnew} is

$$q(T_{dsnew}) = Q(T_{dsnew}) \quad (2.4.14)$$

found by the same method as (2.2.11). The finite difference form, equation (2.3.4), is now employed

$$dQ/dT = (q(T_{dsnew}) - q_{vs}) / \Delta T \quad (2.4.15)$$

From equation (2.3.5)

$$\delta\theta_s = [\theta_s - (\theta_s + (L_v/C_p)q_{vs})] / [1 + (L_v/C_p)dQ/dT] \quad (2.4.16)$$

If $\delta\theta_s$ is less than some tolerance level then q_{1c} may be found by

$$q_{1c} = q_t - q_{vs} \quad (2.4.17)$$

Otherwise, equations (2.4.11) to (2.4.16) are repeated with

$$\theta_{snew} = \theta_{sold} + \delta\theta_s \quad (2.4.18)$$

until q_{1c} is found.

If $0 < z_c < z_b$ then a cloud is formed in the model and no

fog is present. Then, the triangle rule illustrated by Figure 2.3.1 applies. The equation used to handle both fog and no fog cases is

$$q_{1i} = 0.5d_c(q_{1b} + q_{1c}) \quad (2.4.19)$$

The difference between the value of q_{1i} calculated in (2.4.19) and the value of q_{1i} measured by the satellite is then checked to see if it is below an acceptable tolerance value. If it is not, then a regula falsi routine is used to calculate a new value of z_b and equations (2.4.3) to (2.4.19) are repeated until an acceptable value is achieved. Once this occurs, the boundary layer profiles of Θ_e and q_e are found. It is then possible to begin the calculations to derive the surface fluxes of momentum, heat, and moisture, which is the topic of the next section.

2.5 CALCULATION OF SURFACE FLUXES

The calculation of the surface fluxes of momentum, heat, and moisture may now be done. As discussed in the first chapter, satellite measurements of both a neutral

wind speed at some height and a friction velocity may be calculated by means of empirical formulas. Because the debate continues on which is a more appropriate measurement in its correspondence to the measured backscatter, I have chosen to allow the use of either in the model. With the addition of satellite measured sea surface temperature, the surface fluxes may be found.

By following the method of Liu, *et al.* (1979), the surface fluxes may be estimated by first finding u_* and z_0 . Then, the roughness Reynolds number is computed from which z_t and z_q are found. With the addition of the sea surface temperature and mixing ratio, the surface fluxes may be found by using the bulk aerodynamic formulas and the Businger-Dyer unstable diabatic profiles.

For input involving a neutral stability wind, Kondo's (1975) relation is used

$$C_{dn} = p + q(u_{10n})^r \quad (2.5.1)$$

Where p , q , and r are constants which vary for wind speed velocities between 0.3 and 50.0 m/s. Kondo's relation was chosen because of its ability to cover large ranges of wind speed. This allows the model to incorporate cases such as California coastal stratus which do not exhibit

the large air-sea temperature differences common for cold air outbreak; thus, creating a near neutral atmospheric stability.

Equation (2.5.1) may be expressed as

$$(u_*/u_{10n})^2 = p + q[(u_*/k) \ln(10/z_0)] \quad (2.5.2)$$

where I have used

$$C_{dn} = (u_*/u_{10n})^2 \quad (2.5.3a)$$

$$u_{10n} = (u_*/k) (\ln(10/z_0)) \quad (2.5.3b)$$

One may calculate the friction velocity, u_* , by

$$u_* = (C_{dn} (u_{10n}^2))^{1/2} \quad (2.5.4)$$

The roughness length, z_0 , may be found from the expression for u_{10n} in equation (2.5.3b).

$$z_0 = 10 / [\exp((u_{10n}k)/u_*)] \quad (2.5.5)$$

For input involving satellite derived friction

velocity, Charnock's (1955) relation is used to find the roughness length. The equation is

$$z_0 = a(u_*)^2/g \quad (2.5.6)$$

where g is the gravitational acceleration and a is Charnock's constant. Wu (1969) in his study of sea surface roughness, found $a=0.0156$ to be a reasonable value for a large range of oceanic data.

Following the method of Liu, et al. (1979) the roughness Reynolds number is expressed as

$$R_r = z_0 u_* / \nu \quad (2.5.7)$$

where ν is the kinematic viscosity.

According to Liu, et al. (1979), the variables z_t and z_q may be expressed in terms of the roughness Reynolds number by

$$z_t = (a_1 R_r^{0.1} \nu) / u_* \quad (2.5.8)$$

and

$$z_q = (a_2 R_r^{b_2} \psi) / u_* \quad (2.5.9)$$

where the coefficients a_1 , b_1 , a_2 , and b_2 for different ranges of R_r are shown in Table 2.5.1, taken from Liu, et al. (1979).

The distribution of velocity, temperature, and humidity for the surface layer, outside of the region where molecular effects dominate, are governed by the Businger profiles

$$(u - u_0) / u_* = [\ln(z/z_0) - \psi_u] / k \quad (2.5.10)$$

$$(\theta - \theta_0) / \theta_* = [\ln(z/z_t) - \psi_t] / \alpha_h k \quad (2.5.11)$$

$$(q - q_0) / q_* = [\ln(z/z_q) - \psi_q] / \alpha_e k \quad (2.5.12)$$

The diabatic terms, ψ_u , ψ_t , and ψ_q are given by

$$\begin{aligned} \psi_u = & 2 \ln\{[1 + (1 - \beta_u(z_0/L))^{1/4}]/2\} + \ln\{[1 + (1 - \beta_u(z_0/L))^{1/2}]/2\} \\ & - 2 \tan^{-1}[(1 - \beta_u(z_0/L))^{1/4}] + \pi/2 \end{aligned} \quad (2.5.13)$$

$$\psi_t = 2 \ln\{[1 + (1 - \beta_t(z_0/L))^{1/2}]/2\} \quad (2.5.14)$$

ORIGINAL PAGE IS
OF POOR QUALITY

Table 2.5.1. Lower Boundary Values of the Logarithmic Profiles $z_t u_* / -a_1 R_r^{b_1}$ and $z_q u_* / -a_2 R_r^{b_2}$

R_r	a_1	b_1	a_2	b_2
0. - 0.11	0.177	0.	0.292	0.
0.11 - 0.825	1.376	0.929	1.808	0.826
0.825 - 3.0	1.026	-0.599	1.393	-0.528
3.0 - 10.0	1.625	-1.018	1.956	-0.870
10.0 - 30.0	4.661	-1.475	4.994	-1.297
30.0 - 100.0	34.904	-2.067	30.790	-1.845

and

$$\psi_q = 2 \ln \{ [1 + (1 - \beta_q (z_q/L))^{1/2}] / 2 \} \quad (2.5.15)$$

respectively. Liu, et al. (1979) used $k=0.4$, $1/(\alpha_h k) = 1/(\alpha_e k) = 2.2$, and $\beta_u = \beta_t = \beta_q = 16$.

To include the effects of the buoyancy of water vapor, the Obukhov length, L , may be expressed in terms of the virtual potential temperature flux

$$L = (\theta_v u_*^2) / (gk \theta_{v*}) \quad (2.5.16)$$

where θ_v comes from equation (2.2.14)

$$\theta_v = \theta_1 (1 + (1/\epsilon - 1) q_t) \quad (2.5.17)$$

and θ_{v*} is expressed as

$$\theta_{v*} = \theta_* (1 - (1/\epsilon - 1) q_t) + (1/\epsilon - 1) \theta q_* \quad (2.5.18)$$

The profiles (2.5.10) to (2.5.12) are formulated in terms of mean quantities for the boundary layer. These mean values can be associated with the surface flux profiles. Near the surface, mechanical shear dominates

and large gradients may exist in the mean profiles. Higher up, buoyancy begins to dominate and the shears gradually vanish as the profiles approach their mixed layer mean values.

If a matching height, h , is introduced it is possible to solve the problem of matching the mean mixed layer profiles with the surface layer profiles (Wynngaard, et al., 1974). Let h be the height at which the profiles (2.5.10)-(2.5.12) produce the mixed layer mean values. Then one may write

$$\ln(h/z_0) - \psi_u(h/L) = \ln(-h/L) - \psi_u(-h/L) - \ln(-z_0/L)$$

$$\ln(h/z_t) - \psi_t(h/L) = \ln(-h/L) - \psi_t(-h/L) - \ln(-z_t/L) \quad (2.5.19)$$

$$\ln(h/z_q) - \psi_q(h/L) = \ln(-h/L) - \psi_q(-h/L) - \ln(-z_q/L)$$

The height at which the gradients become vanishingly small is determined by the relative importance of shear and buoyant production of turbulence kinetic energy and thus h should be proportional to $-L$ (Wynngaard, et al., 1974). Therefore,

$$K_u = \ln(-h/L) - \psi_u(-h/L)$$

$$K_t = \ln(-h/L) - \psi_t(-h/L) \quad (2.5.20)$$

$$K_q = \ln(-h/L) - \psi_q(-h/L)$$

are constants and the profiles (2.5.10)-(2.5.12) may be expressed as

$$(u-u_0)/u_* = [K_u - \ln(-z_0/L)]/k \quad (2.5.21)$$

$$(\theta - \theta_0)/\theta_* = [K_t - \ln(-z_t/L)]/\alpha_h k \quad (2.5.22)$$

$$(q-q_0)/q_* = [K_q - \ln(-z_q/L)]/\alpha_q k \quad (2.5.23)$$

Wynngaard, et al. (1974) took $-h/L = -10.0$, thus giving $K_u = -0.2$ and $K_t = K_q = -1.02$.

In order to solve equations (2.5.21)-(2.5.23) the Obukhov length, L , must be found. Equations (2.5.16)-(2.5.18) show that it is necessary to know θ_* and q_* in order to do this problem. If an initial guess of θ_{v*} is given and equation (2.5.17) is used to solve for θ_v , the Obukhov length may be determined by equation (2.5.16). The parameter θ_* may be found from equation (2.5.22) and

the satellite measured sea surface temperature θ_0 .

$$\theta_* = (\theta_1 - \theta_0) / [\alpha_h k (K_t - \ln(-z_t/L))] \quad (2.5.24)$$

The sea surface value of the water vapor mixing ratio, q_0 , may be found by using the function $Q(T)$ expressed in equation (2.2.10).

$$q_0 = Q(\theta_0) \quad (2.5.25)$$

Assuming no liquid water or ice is present in the mixed layer where the mean profiles exist, q_t may be used as the value of the water vapor mixing ratio of the mixed layer. Thus, q_* may be found from equation (2.5.23).

$$q_* = (q_t - q_0) / [\alpha_e k (K_q - \ln(-z_q/L))] \quad (2.5.26)$$

A new value of θ_{v*} may now be calculated using equation (2.5.18). The difference between the guessed value and the calculated value of θ_{v*} may be found

$$\Delta\theta_{v*} = \theta_{v*guess} - \theta_{v*calc} \quad (2.5.27)$$

When $\Delta\theta_{v*}$ reaches a small value approximately equal to zero, θ_{v*} has been found, and therefore, the values of θ_* and q_* are known.

The surface fluxes associated with the profiles expressed in equations (2.5.21)-(2.5.23) may be written as

$$\overline{u'w'}|_0 = -u_*^2 \quad (2.5.28)$$

$$\overline{w'\theta'}|_0 = -u_*\theta_* \quad (2.5.29)$$

$$\overline{w'q_t'}|_0 = -u_*q_* \quad (2.5.30)$$

where $\overline{u'w'}|_0$ is the surface flux of momentum, $\overline{w'\theta'}|_0$ is the surface flux of sensible heat, and $\overline{w'q_t'}|_0$ is the surface flux of moisture. Since u_* , θ_* , and q_* are now known, the fluxes may be calculated from these equations.

The method listed above for determining the fluxes assumes unstable conditions. Therefore, a limit must be placed on the calculations for when conditions approach near neutral stability.

As conditions approach near neutral stability, the relation z_0/L goes to zero since L goes to plus or minus infinity. The author chose to limit z_0/L to be

$$(z_0/L)_{\min} \leq -1.0 \times 10^{-7} \quad (2.5.31)$$

By taking a typical value of z_0 over the ocean as 2.0×10^{-4} meters (Miyake, et al., 1970), this gives an upper limit of the Obukhov length of

$$-L = 2000 \text{ meters}$$

The maximum height of z_b in the model is 2000 meters. In order for the Obukhov length not to exceed z_b , the assumption expressed in equation (2.5.31) appears to be a valid lower limit for near neutral stability conditions.

2.6 PARAMETERIZING WATER VAPOR ABOVE THE MABL

A method to parameterize the water vapor content above the MABL is now presented. An analysis is needed in which the profile of q_t above the boundary layer may be found. From this profile, the integrated water vapor content may be found since q_1 is assumed to be zero above z_b . A climatological profile is the easiest means available of accomplishing the analysis. Schemes for both cold air outbreak and California coastal stratus are given

in this section.

2.6.a Cold Air Outbreak

The profile for cold air outbreak was derived from the NASA Mesoscale Air-Sea EXchange (MASEX) project. In order to find the profile of q_t above the boundary layer, profiles of temperature, relative humidity, and mixing ratio were studied. The profiles of temperature and relative humidity were chosen to find the profile of q_t . The mixing ratio profile was discarded because the relative humidity profile seemed more readily adaptable to a wide range of situations.

Given temperature and relative humidity, one may find q_t . So that the profiles studied in MASEX may be made relevant to other cases, the lapse rates of temperature and relative humidity were found. In addition, the mean jump of temperature from the bottom of the inversion to the top of the inversion was calculated along with the mean relative humidity at the inversion top. By using these mean values of $\Delta\theta_z$ and RH, and the lapse rates of θ and RH, the profile above the boundary layer of q_t may be found.

The mean values of $\Delta\theta_z$ and RH are 3 °C and 45%,

respectively. The lapse rates of RH and θ are 8 %/km and 6 °C/km, respectively. By adding $\Delta\theta_t$ to the cloud top temperature and integrating over 10m steps using the lapse rates listed above, q_{v1} above the MABL may be found.

2.6.b California Coastal Stratus

Similarly, a profile for California coastal stratus was computed. Analysis of the profiles found in the studies of Neiburger, et al. (1961) and Meitin (1975) yielded the mean values for this case. Values of $\Delta\theta_t=7^\circ\text{C}$, RH=35%, lapse rate of temperature=6 °C/km, and lapse rate of RH=8 %/km were extracted from the data.

2.7 RADIATIVE FLUX

Given the profiles above the boundary layer, the radiative flux at cloud top may be found by using the flux emissivity method of Staley and Jurica (1970;1972). Since the model assumes no cloud above the boundary layer, the flux at the top of the atmosphere is equal to zero.

The optical path length, $u(z)$, is given by the integration of the water vapor mixing ratio profile.

$$u(z) = \int_z^{z_{top}} (q/g) dp \quad (2.7.1)$$

In equation (2.7.1), z_{top} refers to the highest sounding level available. The flux emissivity $\mathcal{E}(u)$ is found by the interpolation of the values tabulated by Staley and Jurica; thus, giving the downward radiative temperature flux as

$$F = (\sigma / \rho C_p) \int_{z_0}^{z_{top}} T^4 d\mathcal{E}(u(z)) \quad (2.7.2)$$

since the atmosphere is assumed to be cloud free above the MABL.

The method described above, or any other similar radiation model, will yield a value for the radiative temperature flux. Due to the uncertainties involved when using mean profiles in place of actual profiles, the radiative temperature fluxes calculated by the model are not yet reliable. When a better method of finding the profile of water vapor above the MABL is found, the radiative flux method listed above will be useful.

ORIGINAL PAGE IS
OF POOR QUALITY

CHAPTER 3 : COMPUTATIONAL FORM OF THE MODEL

3.1 INTRODUCTION

The computational form of the model is discussed in this chapter. The equations for the model are given in Chapter 2; hence, this chapter references the equations instead of repeating them. This chapter shows the steps needed to produce estimates of the surface fluxes from the input data.

3.2 THE MODEL

In order to estimate the surface fluxes of momentum, heat, and moisture, the satellite inputs of cloud top temperature, integrated liquid water content, and integrated water vapor content must be converted into z_b and the boundary layer profiles of θ_e and q_t . First a guess of the boundary layer height is given. Then, the integrated water vapor content outside of the boundary layer is found by the method in Section 2.6. Then, the method given in Section 2.4 is used to calculate θ_e , q_t ,

and z_b . The integrated liquid water is calculated from the values found in Section 2.4. This calculated value is then compared to the satellite measured value. If the difference between the measured and calculated values of q_{11} is approximately equal to zero, the model continues. Otherwise, a regula falsi routine is used to obtain a new value of the boundary layer height, and the process above is repeated until the difference between the measured and calculated q_{11} 's is approximately equal to zero.

Upon finding the values of θ_* , q_t , and z_b , the model continues. If a neutral wind speed is provided, the model calculates the friction velocity and roughness length by the method shown in equations (2.5.1) to (2.5.5). On the other hand, if a friction velocity is given, the roughness length is calculated by equation (2.5.6). With the values of u_* and z_0 , and following the method of Liu, et al. (1979), a roughness Reynolds number may be computed. This is accomplished by equations (2.5.7) to (2.5.9).

The last satellite measured value, the sea surface temperature, is now used. Values of θ_* and q_* must be found so that the fluxes may be computed. From θ_* and q_t , θ_1 is found. The quantity $(\theta_1 - \theta_0)$ is used for the computation of θ_* . The quantity $(q_t - q_0)$, where q_0 is found from the sea surface temperature, is used for

calculating q_* . With an initial guess of θ_{v*} , equations (2.5.16) to (2.5.18) and equations (2.5.24) to (2.5.25) are employed to calculate θ_* and q_* . Then θ_{v*} is computed by equation (2.5.26) and compared to the value of the original guess of θ_{v*} by equation (2.5.27). If the difference is not approximately equal to zero, a regula falsi routine is employed to compute a new θ_{v*} . The process above is repeated until the difference is approximately equal to zero, at which time the model continues.

Finally, with values for u_* , θ_* , and q_* , the surface fluxes of momentum, heat and moisture may be estimated. Equations (2.5.28) to (2.5.30) are used to accomplish this task.

A note about the computations listed above. Original test runs of the model showed that more than one solution existed for each combination of input parameters. Numerically, these solutions were valid; however, these solutions were physically unrealistic due to the extremely high dewpoint temperatures and low mixing ratios encountered. In order to "force" the model to converge to the "realistic" answer the following was done. An upper limit of 2000m for z_b was chosen, since the majority of

the physically unrealistic solutions were at z_b values greater than 2000m. To handle the unrealistic solutions that occurred below 2000m, the initial guesses of z_b for the regula falsi routine were set at 1200 and 100m. Since no double solutions were seen to exist below 1200m, any solutions with z_b less than this height will be accurate. For solutions between 1200 and 2000m, where double solutions might occur, a very restrictive tolerance was placed on q_{11} . Runs of the model showed that q_{11} was extremely sensitive to changes in height. By requiring a near perfect convergence of the measured and calculated integrated liquid water contents, the problem of a possible double solution in the 1200 to 2000m range seems to have been solved.

In this chapter, the computational form of the model has been discussed. The steps needed to estimate the surface fluxes from the original satellite data have been shown. The next chapter deals with the model's results for its test runs.

CHAPTER 4 : MODEL RESULTS

4.1 INTRODUCTION

The results of the test runs of the model are discussed in this chapter. First, the applications of the model are presented. Next, the percent variation of the output parameters with variation of the input parameters is shown. Next, the expected accuracy of the model with respect to current accuracies of satellite measurements is presented. Last, the strengths and weaknesses of the model are discussed.

4.2 MODEL APPLICATIONS

The model was originally developed for the case of cold air outbreak; however, it may also be applied to California coastal stratus. The model assumptions of a horizontally homogeneous, cloud-topped boundary layer with little or no liquid water above the boundary layer apply to both cases mentioned above.

In order to test the model's capabilities, the

routine described in Section 2.3 was run over a large range of values for θ_e , q_t , and z_b . The predicted values of θ_b , q_{li} , and q_{vi} from this routine were then used as input for the model. For the cases in which the routine in Section 2.3 predicted clouds and/or clouds and fog, the model computed values of θ_e , q_t , and z_b which agreed with the variables inputted into the routine. However, for cases in which no clouds were predicted by the routine, the model would not converge to an answer. The routine in Section 2.3 was then run for typical ranges of values for the case of cold air outbreak with θ_e ranging from -30 to 10 °C, q_t ranging from 1.0 to 5.0 g/kg, and z_b ranging from 500 to 2000 meters. The routines predicted values of θ_b , q_{li} , and q_{vi} were then used as the range of values to compute the sensitivities of the output parameters described in the next section.

4.3 VARIATION OF INPUT AND OUTPUT PARAMETERS

The percent variation of the heat and moisture fluxes with variation of u_{10n} , u_* , θ_b , θ_o , q_{li} , and q_{vi} is now presented. The model was tested over the range of values listed above plus the ranges for u_{10n} of 5 to 20 m/s, for u_* of .1 to .7 m/s, and for θ_o of 5 to 20 °C. The

figures presented in this chapter are from one test range of values for the model. The input variables for the cases shown here were held constant, except when they were the variable being tested, at $u_{10n}=10$ m/s, $\theta_b=-15$ °C, $\theta_0=10$ °C, $q_{11}=300$ m g/kg, and $q_{v1}=900$ m g/kg.

The 10m neutral wind speed was tested over the range of 5 to 14 m/s in this case. u_{10n} is related to the surface fluxes through u_* , z_0 , z_t , and z_q . The results of the variation of both the heat and moisture fluxes with respect to u_{10n} is nearly linear. Analysis shows that with a +/-10% variation in u_{10n} resulting in a +/-10% variation in both the heat and moisture fluxes.

The friction velocity was tested next with a range of .2 to .65 m/s in this case. The friction velocity is directly related to the fluxes as well as through z_0 , z_t , and z_q . The results of the tests showed the variation is, as in the case of u_{10n} , nearly linear. Analysis of the results shows that a +/-10% variation in u_* produces a +/-9% variation in both the heat and moisture fluxes.

Next, the cloud top temperature was tested over a range of -15 to -10.5 °C in this case. The cloud top temperature is related to the heat and moisture fluxes through θ_1 and q_t . Results for the variation of the heat

flux may be seen in Figure 4.3.1.

As seen in Figure 4.3.1, the heat flux decreases for increasing θ_b . The change in slope of the curve is due to the presence of fog predicted by the model. Because of the uncertainty of the model's evaluation of fluxes under foggy conditions, only cases in which no fog is present were considered for error determinations. The error for the no fog portion of this case as well as in all other cases is for a $\pm 1^\circ\text{C}$ change in θ_b , the heat flux varies by $\pm 4\%$. Figure 4.3.2 shows the variation of the moisture flux with θ_b .

As can be seen in the figure, the moisture flux also decreases with increasing θ_b . The change in slope of the curve seen in the figure corresponds with the formation of fog. The results for a $\pm 1^\circ\text{C}$ change in θ_b , in the no fog cases, are a $\pm 4.5\%$ variation in the moisture flux.

Sea surface temperature was the next variable tested. The range in this case was from 5 to 14°C . Sea surface temperature affects the heat flux directly and the moisture flux through q_0 . Figures 4.3.3 and 4.3.4 show the variations of heat and moisture fluxes, respectively.

As shown in the figures, both the heat and moisture fluxes increase with increasing θ_0 . For a $\pm 1^\circ\text{C}$ change of θ_0 , the heat flux varies $\pm 3\%$, and the moisture flux

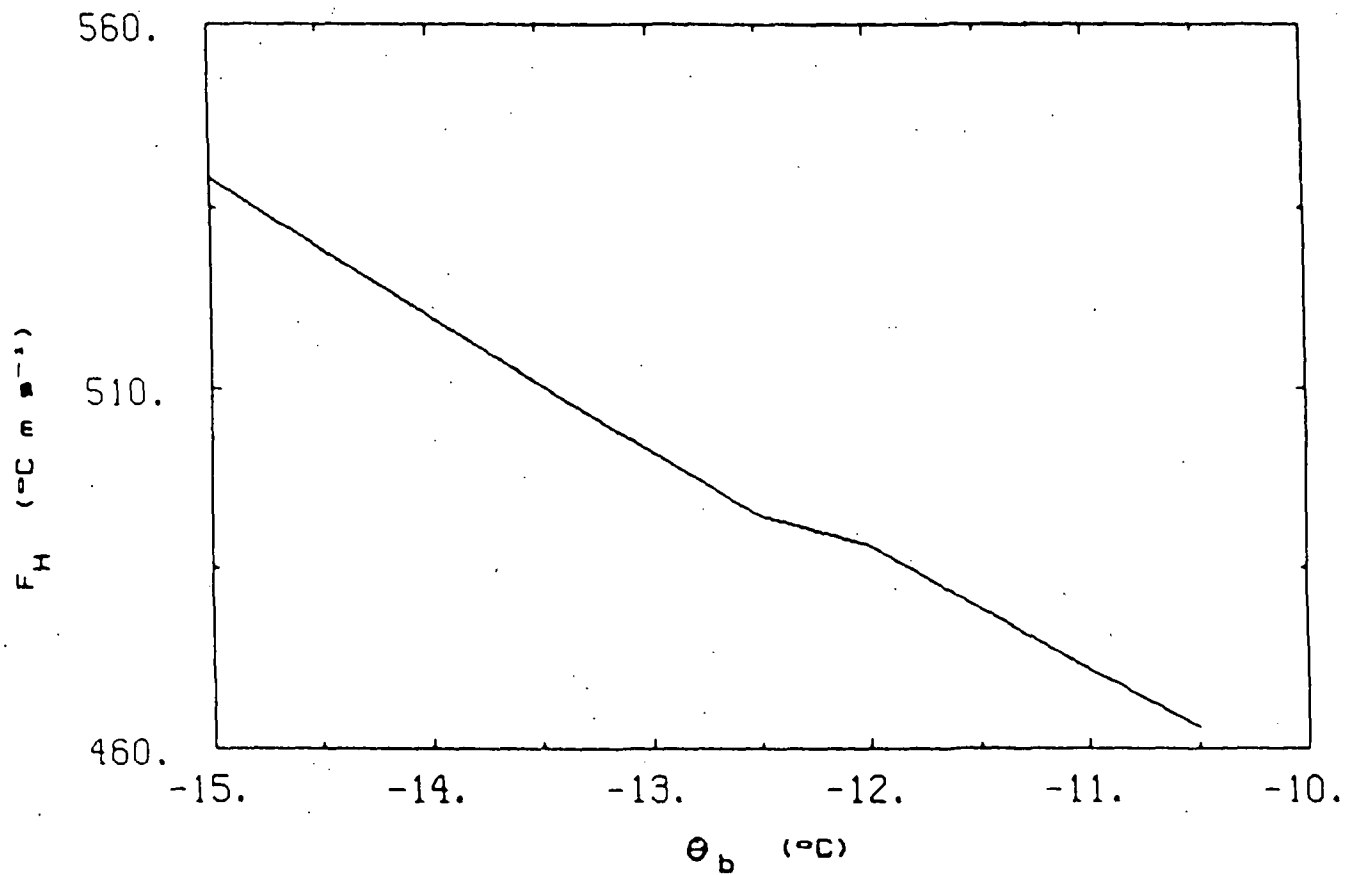


Figure 4.3.1. Variation of Heat Flux with Cloud Top Temperature

ORIGINAL PAGE IS
OF POOR QUALITY

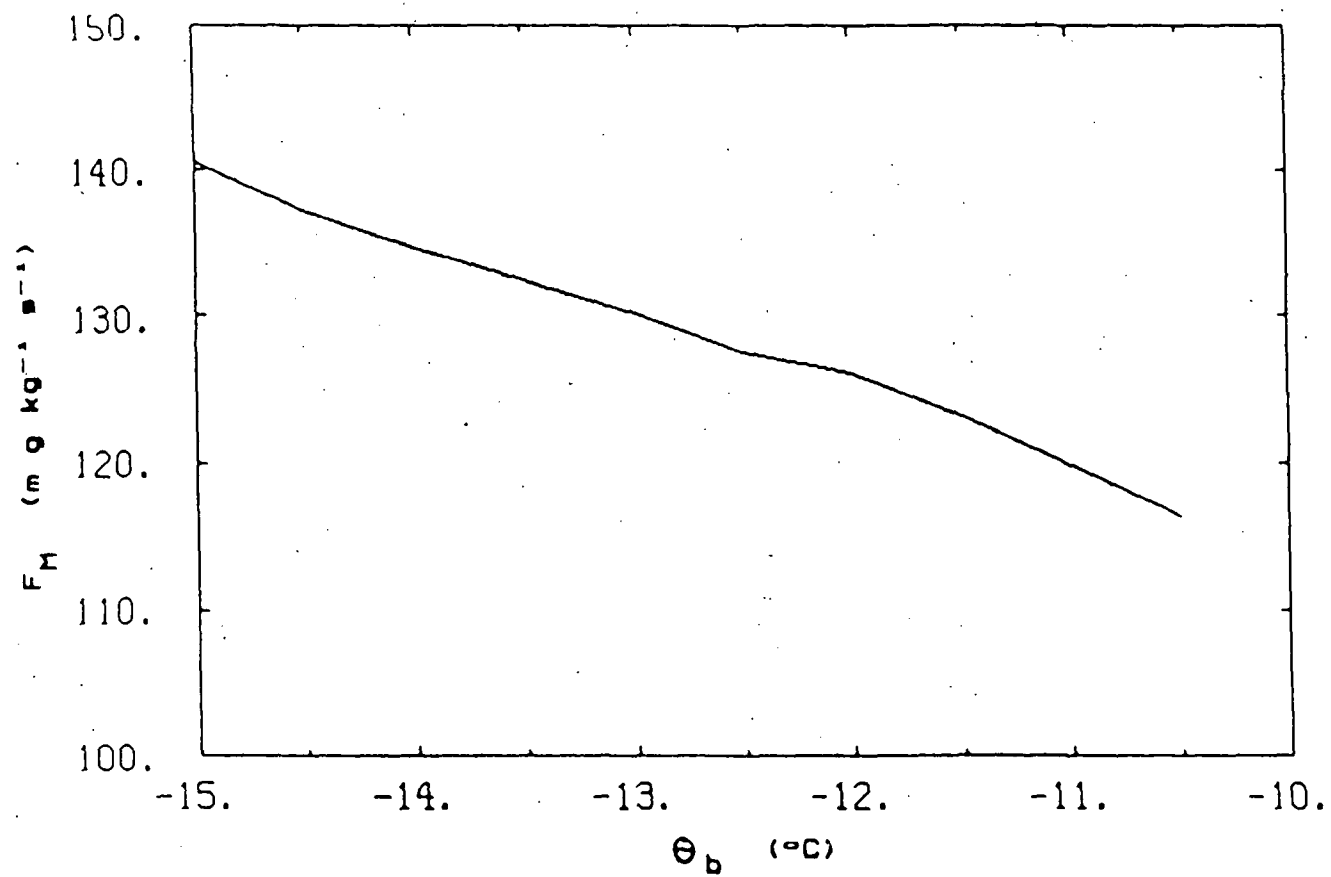


Figure 4.3.2. Variation of Moisture Flux with Cloud Top Temperature

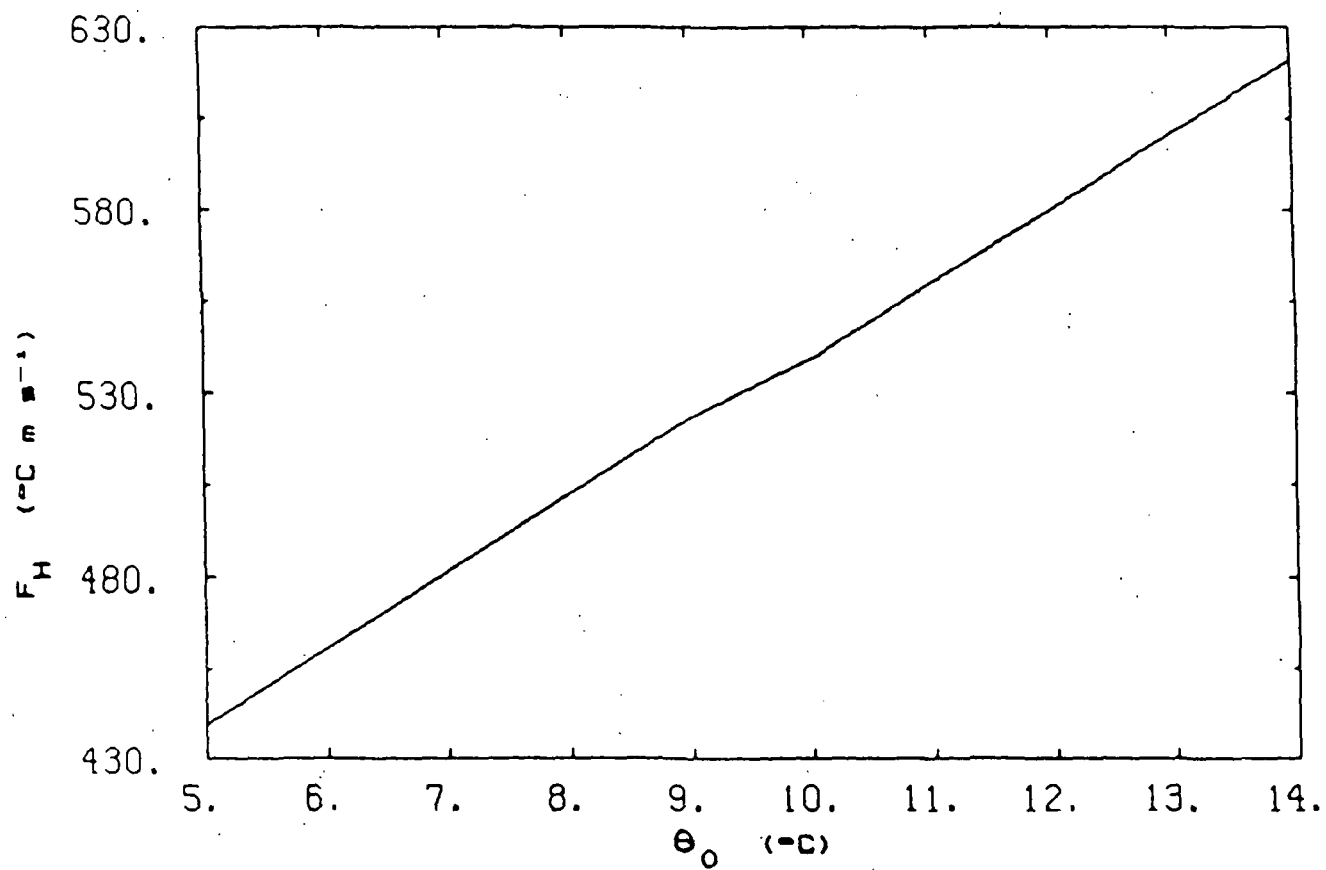


Figure 4.3.3. Variation of Heat Flux with Sea Surface Temperature

ORIGINAL PAGE IS
OF POOR QUALITY

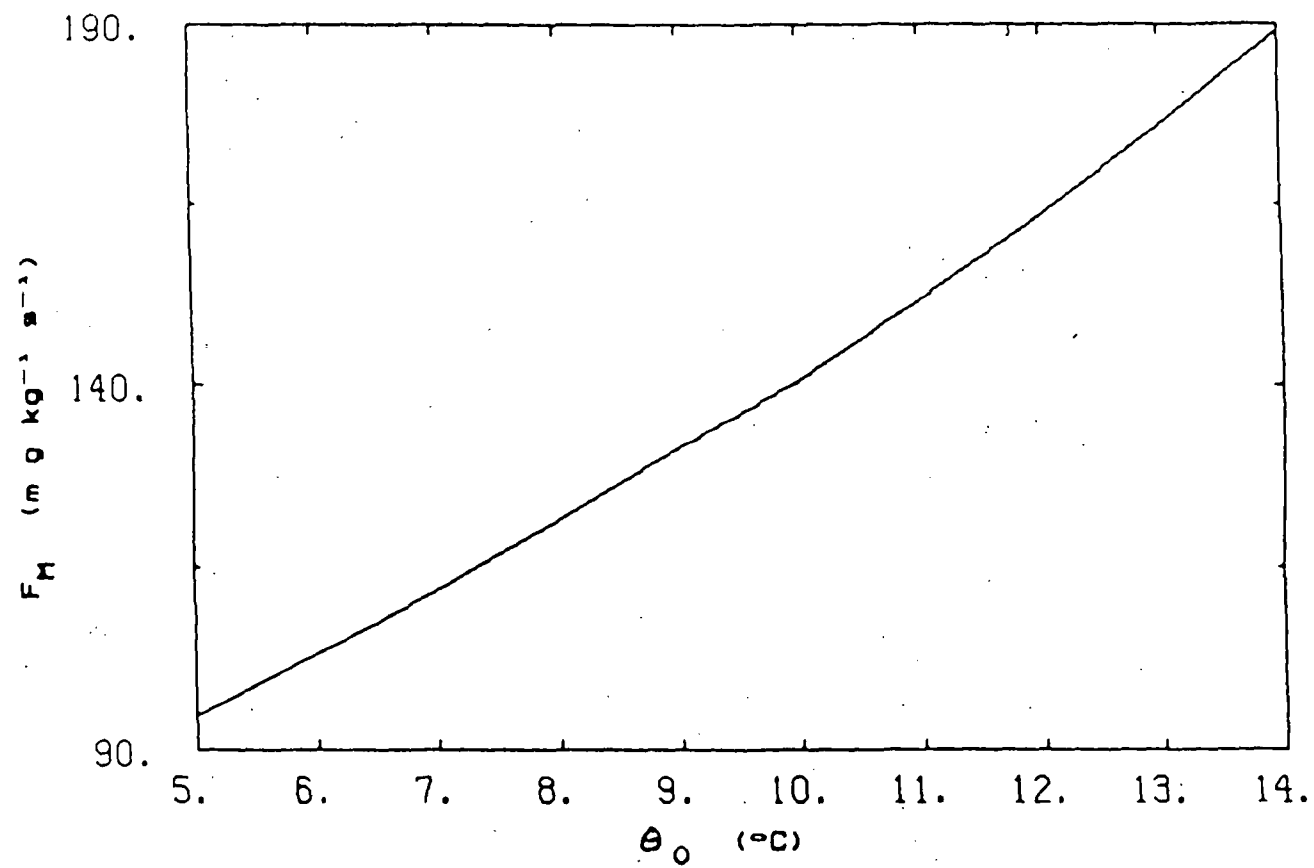


Figure 4.3.4. Variation of Moisture Flux with Sea Surface Temperature

varies $\pm 7\%$.

Next, the integrated liquid water content was tested over the range of 300 to 480 m g/kg, for this case. The integrated liquid water content effects the heat flux through θ_1 and the moisture flux through q_t . Figure 4.3.5 shows the variation of the heat flux, and Figure 4.3.6 shows the variation of the moisture flux.

As can be seen in Figure 4.3.5, the heat flux increases with increasing q_{11} . Analysis shows that for a ± 100 m g/kg change in q_{11} , the heat flux changes $\pm 0.25\%$. However, in Figure 4.3.6, one may see that the moisture flux decreases with increasing q_{11} . A ± 100 m g/kg change in q_{11} produces a $\pm 3.5\%$ change in the moisture flux.

Figures 4.3.7 and 4.3.8 show the variation of the heat and moisture fluxes with varying integrated water vapor content. The integrated water vapor was varied from 720 to 900 m g/kg, for this case. The heat and moisture fluxes are effected by q_{v1} through θ_1 and q_t , respectively.

As shown in the figures, the heat flux decreases and the moisture flux increases with increasing q_{v1} . Analysis shows that for a ± 100 m g/kg change in q_{v1} , the heat flux

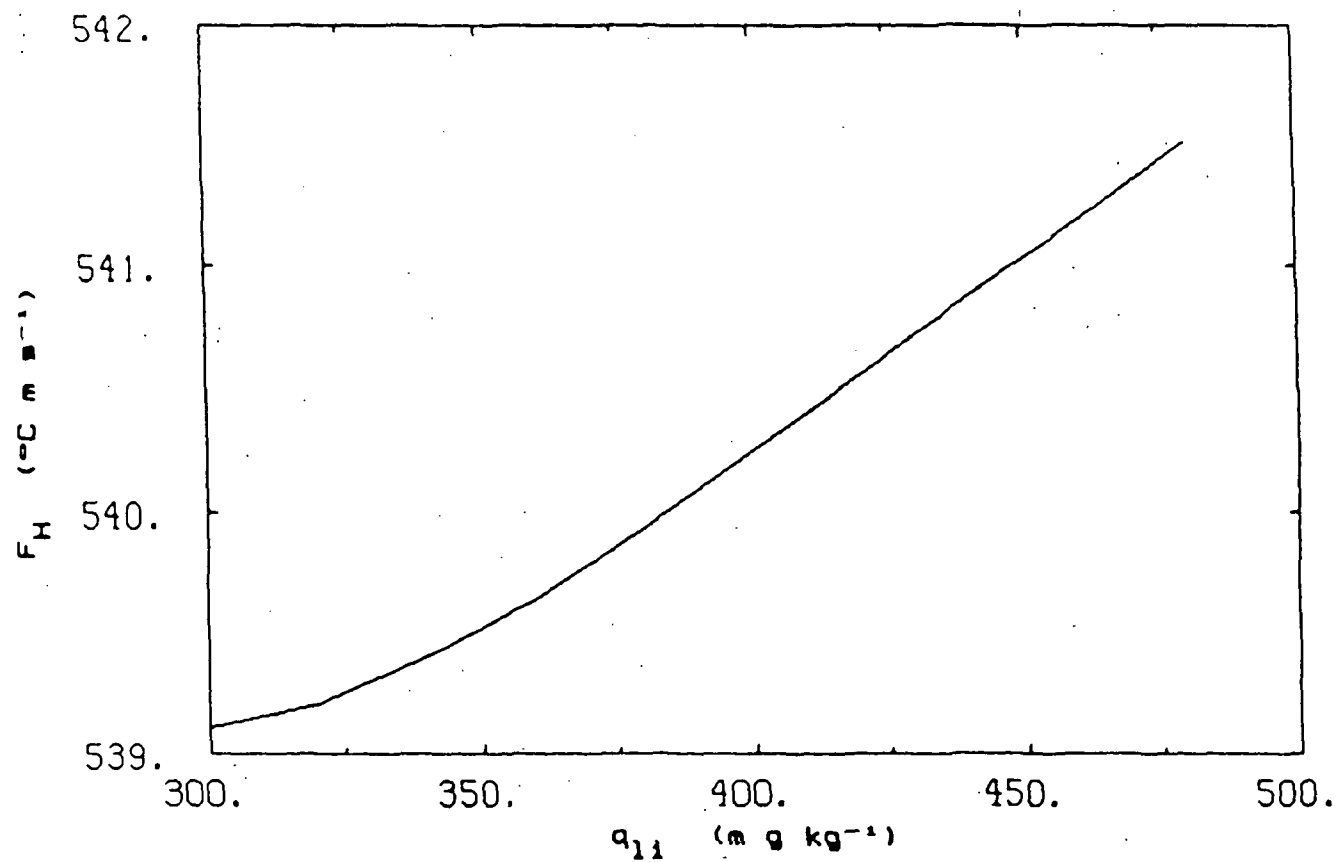


Figure 4.3.5. Variation of Heat Flux with Integrated Liquid Water Content

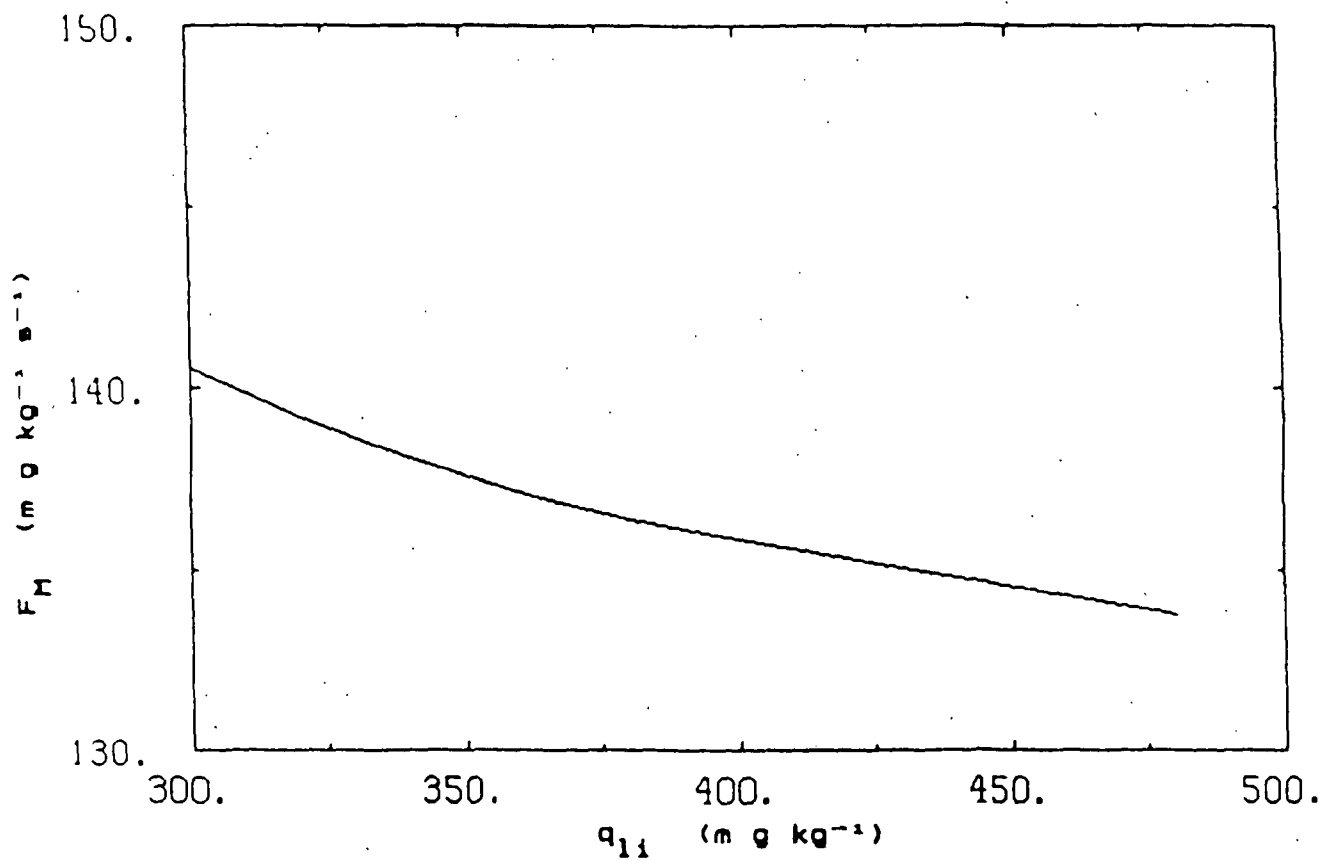


Figure 4.3.6. Variation of Moisture Flux with Integrated Liquid Water Content

ORIGINAL PAGE IS
OF POOR QUALITY

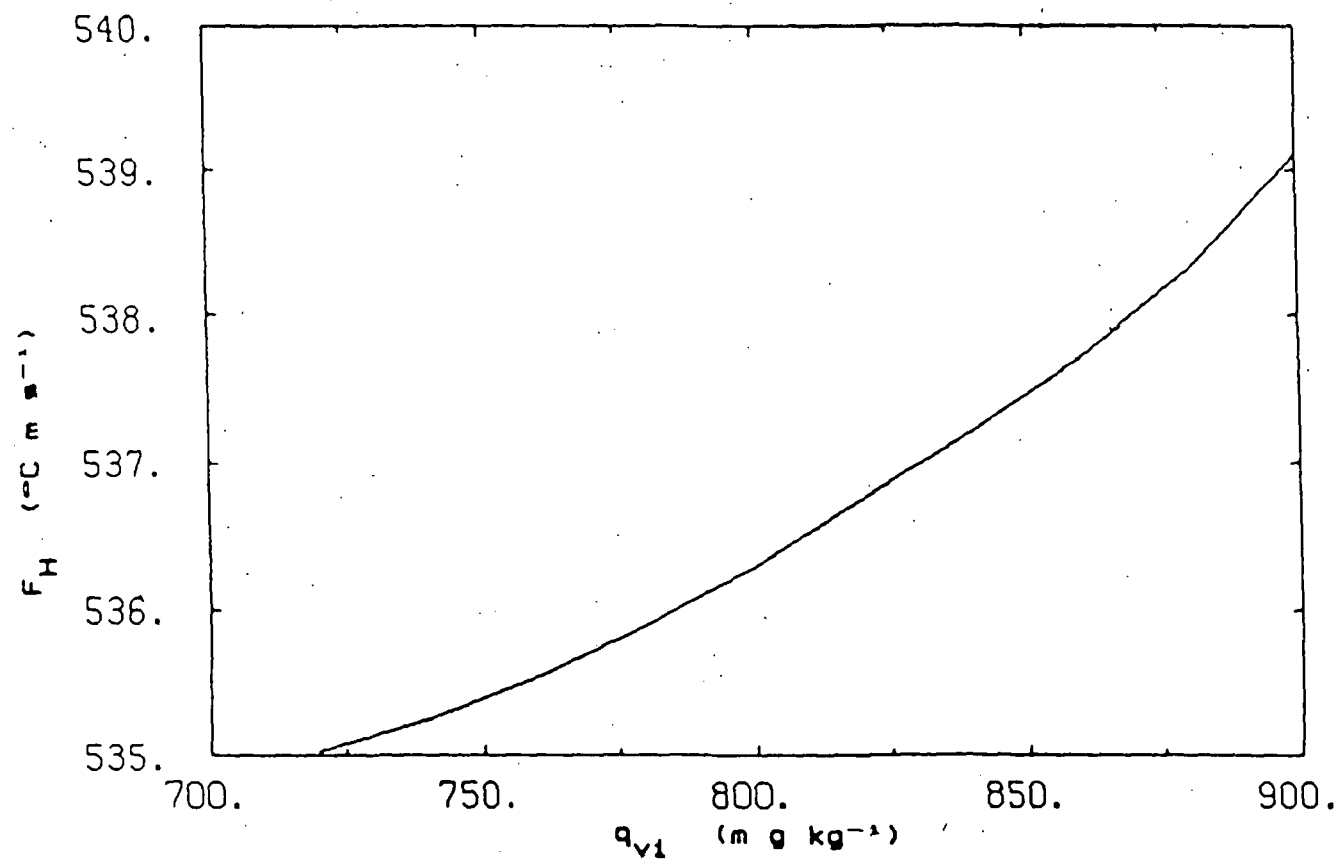


Figure 4.3.7. Variation of Heat Flux with Integrated Water Vapor Content

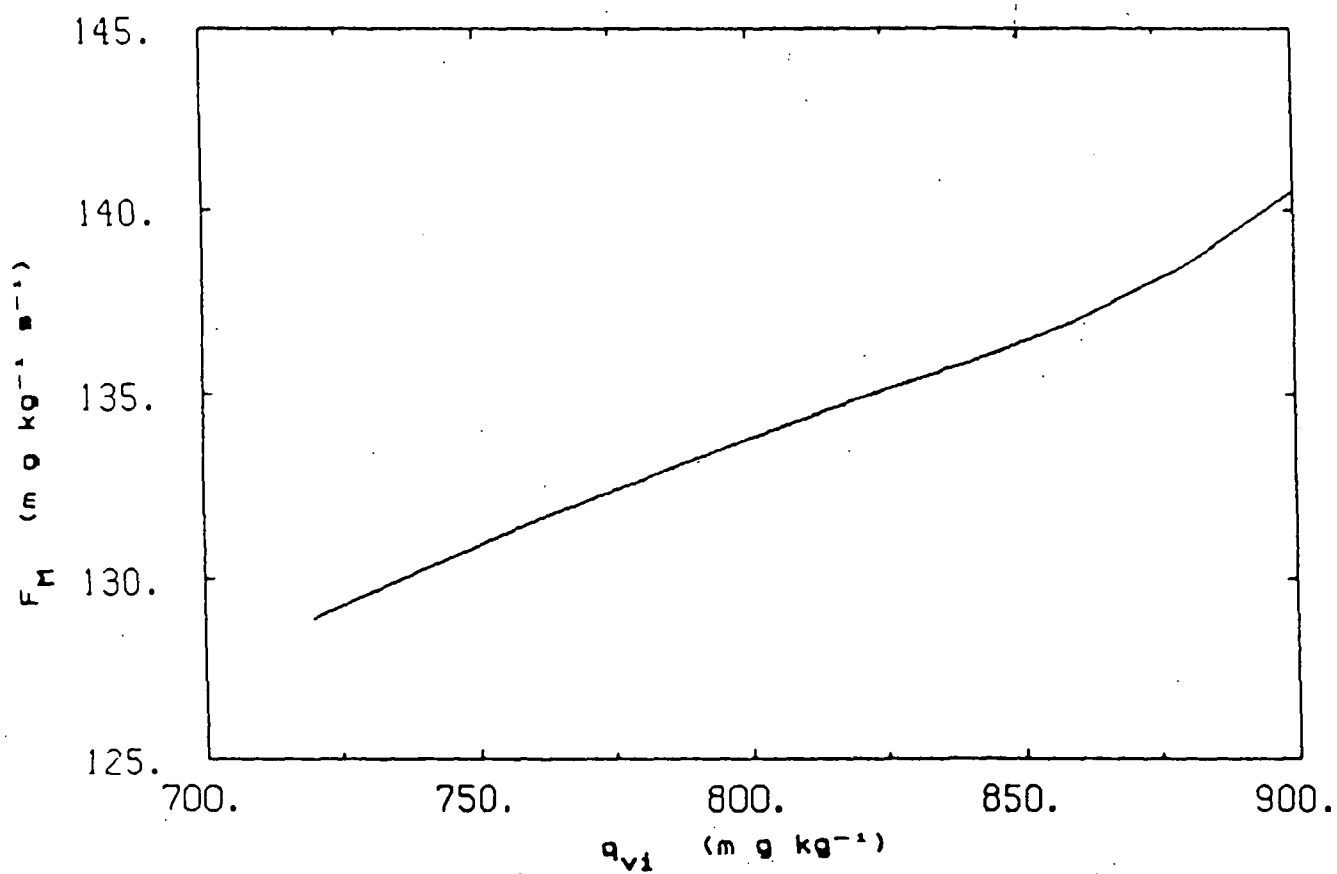


Figure 4.3.8. Variation of Moisture Flux with Integrated Water Vapor Content.

varies $\pm 0.6\%$ and the moisture flux varies $\pm 5\%$.

4.4 EXPECTED MODEL ACCURACIES WITH SATELLITE DATA

The expected model accuracies with current satellite technology is now presented. Through infrared measurements, the cloud top temperature may be found within $\pm 2^\circ\text{C}$. The accuracies of the sea surface temperature, the 10m neutral wind speed, and the friction velocity are $\pm 1.5^\circ\text{C}$, $\pm 2\text{m/s}$ or 20%, and $\pm 20\%$, respectively (Satellite Microwave Remote Sensing, edited by T.D. Allan, 1983). These values were obtained from results of SEABAT and NIMBUS 7 data analysis. The expected retrieval errors of the integrated liquid and water vapor contents for the SMMR package on NIMBUS 5 are $\pm 650\text{m g/kg}$ and $\pm 1500\text{m g/kg}$, respectively (Chang and Wilheit, 1979).

By applying these accuracies to the percent variations of the model discussed in the previous section, the expected accuracy of the model may be found. Since the difference of the variations with respect to u_{10n} and u_* is 1%, the larger of the two errors will be used.

Given a 20% error in satellite derived u_{10n} , the model will produce a 20% error in both the heat and

moisture fluxes. A 2 °C error in θ_b produces a 8% error in the heat flux and a 9% error in the moisture flux. An error of 1.5 °C in the sea surface temperature gives a 4.5% error in the heat flux and an 6.75% error in the moisture flux. A 650m g/kg error in q_{li} produces a 1.6% error in the heat flux and a 22.75% error in the moisture flux. An error of 1500m g/kg for q_{vi} gives a 9% error in the heat flux and a 75% error in the moisture flux. Taking these errors to be independent of each other, it is possible to compute the expected r.m.s. error of the model. For the errors listed above for each parameter, the expected overall r.m.s. error of the model is 24% for the heat flux and 82% for the moisture flux (See Table 4.4.1). Although these errors are quite high, it must be understood that the satellite technology which allows the measurements of the necessary parameters is still in its infancy. The major errors in the model may be attributed to the calculations of q_{li} and q_{vi} . Future improvement in the algorithms used to find these parameters would significantly improve this model's estimates of the surface fluxes.

Table 4.4.1. Individual Expected Errors due to Each Satellite Parameter and Total Expected Model Error

PARAMETER	SATELLITE RMS ERRORS	HEAT	MOISTURE
u_{10n}	20%	20%	20%
θ_b	2.0 °C	8%	9%
θ_o	1.5 °C	4.5%	6.75%
q_{11}	650 m g/kg	1.6%	22.75%
q_{v1}	1500 m g/kg	9%	75%

Total Expected R.M.S. Errors: 24% 82%

4.5 STRENGTHS AND WEAKNESSES

The model's strengths and weaknesses are now discussed. The model handles well in cloudy and cloudy with fog conditions. The model is extremely quick, and, given reasonable input accuracies, will produce reasonable estimates of the surface fluxes. As far as the author can tell, the model is the only one currently available which will provide estimates of the surface fluxes for a cloud topped MABL from satellite measurable parameters.

On the other hand, the model is not capable of calculating the surface fluxes when a cloud is not present. The calculation of the fluxes is also unclear when gaps in the clouds are present. If the gaps are large enough, the calculation of the cloud top temperature becomes difficult, and the profiles assumed in the model break down. The model's assumption that the cloud top is also the base of the inversion is not always correct. The cloud may extend into the inversion layer; however, due to the uncertainty of how far into the cloud the infrared cloud top temperature is actually being measured, this weakness may be corrected. The presence of fog below the cloud layer also presents a problem due to the

uncertainty of how the model's equations react to fog. The main weakness of the model is the parameterization of the water vapor above the boundary layer. The mean values chosen are not representative of all possible cases, and further work in this area is needed.

CHAPTER 5 : CONCLUSIONS

In conclusion, this thesis has produced a viable model to estimate the surface fluxes from satellite measurable parameters. The model applies to cases of cold air outbreak, California coastal stratus, or to any cloud topped MABL which has a sufficiently strong heat flux or cloud top radiative cooling to cause the potential temperature and total water profiles of the layer to be well-mixed. With improvements of the current satellite technology, this model will provide accurate estimates of the surface fluxes. The model is relatively simple and extremely quick running. The model is also the only one of its kind currently available to estimate the surface fluxes of momentum, heat, and moisture of the cloud topped marine atmospheric boundary layer from satellite measurable parameters.

In light of this thesis, some areas of further research are suggested. More work is necessary to find a method of parameterizing the water vapor content above the MABL. More research is also necessary for testing the model for the case of California coastal stratus to see

how well it reacts under nearly neutral conditions. The evaluation of the surface fluxes under foggy conditions and how well the model handles them is another area for study. The problem of gaps in the cloud deck and a method to handle this is an area for further thought. Also, other possible sets of parameters should be examined to see if a better method than the one presented may be found.

REFERENCES

- Agee, E.M., and R.P. Howley, 1977. Latent and Sensible Heat Flux Calculations at the Air-Sea Interface during AMTEX 74. J. Appl. Meteor., 16, 443-447.
- Chang, A.T.C., and T. Wilhelm, 1979. Remote Sensing of Atmospheric Water Vapor, Liquid Water, and Wind Speed of the Ocean Surface by Passive Microwave Techniques from the NIMBUS 5 Satellite. Radio Sci., 14, 793-802.
- Charnock, H., 1955. Wind Stress on a Water Surface. Quart. J. Roy. Meteor. Soc., 81, 639.
- Chou, B.H., and D. Atlas, 1982. Satellite Estimates of Ocean-Air Heat Fluxes During Cold Air Outbreak. Mon. Wea. Rev., 110, 1434-1450.
- Kondo, J., 1975. Air-Sea Bulk Transfer Coefficients in Diabatic Conditions. Bound. Layer Meteor., 9, 91-112.
- Liu, W.T., et al., 1979. Bulk Parameterization of the Air-Sea Exchanges of Heat and Water Vapor Including the Molecular Constraints at the Interface. J. Atmos. Sci., 36, 1722-1735.
- Maitin, R., 1975. A Case Study of a Marine Inversion on the Oregon Coast. M.S. Thesis, Department of Meteorology, Florida State University, Tallahassee, Florida, 109pp.
- Miyake, M., et al., 1970. Comparison of Turbulent Fluxes over Water Determined by Profile and Eddy Correlation Techniques. Quart. J. Roy. Meteor. Soc., 96, 132-137.
- Neiburger, M., et al., 1961. Studies of the Structure of the Atmosphere over the Eastern Pacific Ocean in Summer: I. The Inversion over the Eastern North Pacific Ocean. Univ. of California Press, 94pp.
- Satellite Microwave Remote Sensing, edited by T.D. Allan, Ellis Horwood Limited, West Sussex, England, 1983, 526pp.

- Stage, S.A., 1979. A Model for Modification of the Cloud-Topped Marine Boundary Layer over Water. Ph.D. Thesis, University of Washington, Seattle, Washington, 281pp.
- Stage, S.A., 1983. Boundary Layer Evolution in the Region between Shore and Cloud Edge during Cold Air Outbreaks. *J. Atmos. Sci.*, **40**, 269-287.
- Stage, S.A., and J.A. Businger, 1981a. A Model for Entrainment into a Cloud-Topped Marine Boundary Layer, Part I: Model Description and Application to a Cold Air Outbreak Episode. *J. Atmos. Sci.*, **38**, 2213-2229.
- Stage, S.A., and J.A. Businger, 1981b. A Model for Entrainment into a Cloud-Topped Marine Boundary Layer, Part II: Discussion of Model Behavior and Comparison with other Models. *J. Atmos. Sci.*, **38**, 2230-2242.
- Staley, D.O., and G.M. Jurica, 1970. Flux Emissivity Tables for Water Vapor, Carbon Dioxide and Ozone. *J. Appl. Meteor.*, **9**, 365-372.
- Staley, D.O., and G.M. Jurica, 1972. Effective Atmospheric Emissivity under Clear Skies. *J. Appl. Meteor.*, **11**, 349-356.
- Wu, J., 1969. Wind Stress and Surface Roughness at Air-Sea Interface. *J. Geophys. Res.*, **74**, 444-455.
- Wyngaard, J.C., et al., 1974. Some Aspects of the Structure of Convective Planetary Boundary Layers. *J. Atmos. Sci.*, **31**, 747-754.